

Trinucleon form factors with relativistic multirank separable kernels

Serge Bondarenko^a, Valery Burov^a, Sergey Yurev^a

^a*BLTP, Joint Institute for Nuclear Research, Dubna, 141980, Russia*

Abstract

This paper studies elastic electron-trinucleon scattering in the relativistic impulse approximation. The amplitudes for a trinucleon have been obtained by solving the relativistic generalization of the Faddeev equations with a multirank separable kernel of the nucleon-nucleon interactions. The static approximation and additional relativistic corrections for the trinucleon electromagnetic form factors have been calculated for the momentum transfer squared up to 50 fm^{-2} .

Keywords:

Elastic electron-trinucleon scattering, Bethe-Salpeter equation, Faddeev equation, relativistic approach

1. Introduction

In the previous article [1] we used the solutions of the Bethe-Salpeter-Faddeev equation (BSF) with the rank-one Yamaguchi and Tabakin separable kernels of the nucleon-nucleon (NN) interactions to calculate the ^3He charge form factor (F_C). Two approximations were considered: the static approximation (SA) and relativistic corrections (RC). The choice of the simple rank-one kernel did not allow us to reproduce the diffraction minimum of the form factor F_C .

Authors of [2] have found that the calculations with multirank separable NN kernel of interactions in the SA can produce the first diffraction minimum of the form factor F_C although at the higher value of the momentum transfer.

Email address: `bondarenko@jinr.ru` (Serge Bondarenko)

But nevertheless, this article has focused us on the idea that the RC can move the first diffraction minimum closer to the one experimentally observed.

In the current paper we have considered several multirank kernels: purely phenomenological covariant generalization of the nonrelativistic (NR) Graz-II [3] potential and the derived one from separable approximation of the Paris [4, 5] NN potential. The parameters of the NR separable kernels were refitted in [2] to use them in the Bethe-Salpeter approach.

Today there are several relativistic approaches known to calculate trinucleon form factors (see, review [6]). The first one is the conventional approach: it views the nucleus as made up of nucleons interacting among themselves (via two- and many-body realistic potentials), and with external electromagnetic (EM) fields (via one- and many-body currents), including relativistic corrections. The second approach is the chiral effective field theory (ChEFT) which uses the methods of quantum field theory with Lagrangian including the nucleon, pion and photon fields to obtain one- and many-body EM currents. The third approach applies the covariant spectator theory (CST) to construct the three-nucleon wave function. Within the framework of the latest approach, the corresponding covariant equation is solved by means of the one-boson-exchange kernel of the interactions including several mesons.

One should also mention the light-front relativistic Hamiltonian dynamics (RHD) which takes the three-body forces [7] into account.

The main difference of the BSF formalism from the approaches mentioned above is that all the nucleons of the trinucleon BSF amplitude are off-mass-shell and there are two more free variables p_0, q_0 used in the calculations. These variables introduce additional difficulties in obtaining the solution of the BSF equations and calculating the form factors, namely, the peculiarities in the p_0, q_0 complex plane.

One of the important physical problems in the study of the trinucleon form factors is to describe the right location of the first diffraction minimum. For the ${}^3\text{He}$ and ${}^3\text{H}$ charge and magnetic form factors the result for the conventional and ChEFT approaches successfully reproduces the measured form factors up to momentum transfers squared $t \simeq 9 \text{ fm}^{-2}$. The ChEFT results seem to underestimate the experimental data beyond $t \gtrsim 9 \text{ fm}^{-2}$, in particular, they predict the form factor zeros at significantly lower values of t . On the other hand, the CST calculations are limited to the approximation which omits the interaction current contribution. Therefore, only the isoscalar magnetic contribution should be compared to the experimental

data. For this isoscalar magnetic observable the agreement is good.

The article follows the ideas given in [1] where the rank-one kernels were applied. In contrast to it, in this work the calculations with the multirank relativistic separable kernels of NN interactions Graz-II and Paris have been performed. The results of the calculations better agree with the experimental data than the results obtained with the rank-one kernels – Yamaguchi and Tabakin.

The paper is organized as follows: Sec. 2 gives the expressions for the trinucleon EM form factors, Sec. 3 defines the static approximation and relativistic corrections, Sec. 4 discusses the calculations and results, and, finally, Sec. 5 gives the conclusion.

2. Trinucleon form factors

As a system with one-half spin, the EM current of ${}^3\text{He}$ or ${}^3\text{H}$ can be parameterized by two elastic form factors: charge (electric) F_C and magnetic F_M (see, for example, [8]). In the calculations below, we apply a straightforward relativistic generalization of the NR expressions for the ${}^3\text{He}$ and ${}^3\text{H}$ charge and magnetic form factors [8, 9, 10, 11]:

$$2F_C({}^3\text{He}) = (2F_C^p + F_C^n)F_1 - \frac{2}{3}(F_C^p - F_C^n)F_2, \quad (1)$$

$$F_C({}^3\text{H}) = (2F_C^n + F_C^p)F_1 + \frac{2}{3}(F_C^p - F_C^n)F_2, \quad (2)$$

$$\mu({}^3\text{He})F_M({}^3\text{He}) = \mu_n F_M^n F_1 + \frac{2}{3}(\mu_n F_M^n + \mu_p F_M^p)F_2 + \frac{4}{3}(F_M^p - F_M^n)F_4, \quad (3)$$

$$\mu({}^3\text{H})F_M({}^3\text{H}) = \mu_p F_M^p F_1 + \frac{2}{3}(\mu_n F_M^n + \mu_p F_M^p)F_2 + \frac{4}{3}(F_M^n - F_M^p)F_4, \quad (4)$$

where $F_C^{p,n}$, $F_M^{p,n}$ are the charge and magnetic form factors of the proton and neutron, $\mu({}^3\text{He})$, $\mu({}^3\text{H})$, μ_p , μ_n are magnetic moments of the ${}^3\text{He}$, ${}^3\text{H}$, proton and neutron, respectively.

The functions F_{1-4} can be expressed in terms of the wave functions of the trinucleon which can be represented as linear combinations of the BSF equation solutions with different spin-isospin states [1, 8]:

$$F_1(\hat{Q}) = \int d^4\hat{p} \int d^4\hat{q} G_1'(\hat{k}_1') G_1(\hat{k}_1) G_2(\hat{k}_2) G_3(\hat{k}_3) \sum_{i=1}^3 \Psi_i^*(\hat{p}, \hat{q}; \hat{P}) \Psi_i(\hat{p}, \hat{q}; \hat{P}'),$$

$$\begin{aligned}
F_2(\hat{Q}) &= -3 \int d^4\hat{p} \int d^4\hat{q} G'_1(\hat{k}'_1) G_1(\hat{k}_1) G_2(\hat{k}_2) G_3(\hat{k}_3) \Psi_1^*(\hat{p}, \hat{q}; \hat{P}) \Psi_2(\hat{p}, \hat{q}'; \hat{P}'), \\
F_4(\hat{Q}) &= \int d^4\hat{p} \int d^4\hat{q} G'_1(\hat{k}'_1) G_1(\hat{k}_1) G_2(\hat{k}_2) G_3(\hat{k}_3) \Psi_3^*(\hat{p}, \hat{q}; \hat{P}) \Psi_3(\hat{p}, \hat{q}'; \hat{P}'), \quad (5)
\end{aligned}$$

In our previous work we performed the calculations for the rank-one interaction kernels [1, 12]. There we also analyzed the influence of the type of nucleon form factors on the ${}^3\text{He}$ form factor [12]. In the current paper we deal with the multirank separable kernels Graz-II (with $p_d=4,5,6\%$), Paris-1 and Paris-2.

To calculate the functions F_{1-4} , it is convenient to use the Breit reference system. The solutions of the BSF equation, however, have been found in the c.m. (rest) frames of the corresponding trinucleon. To relate the Breit and initial (final) particle c.m. frames, the Lorentz transformations should be applied to the four-momenta.

Thus, the arguments of the initial and final particle wave functions and propagators were expressed in terms of the momenta calculated in the corresponding c.m. frames and related to each other using the Lorentz transformations.

3. Static approximation and relativistic corrections

Below we remind the general approximations and corrections (see detailed formulae in [1]). Since the solutions of the BSF equations have been obtained in the Euclidean space [13] and are known only for real values of q_4 and p_4 , the simplest way to calculate F_{1-4} is to apply the Wick rotation procedure $p_0 \rightarrow ip_4, q_0 \rightarrow iq_4$, if it is possible. Thus, one needs to investigate the analytic structure of the integrand on the complex-valued variables p_0, q_0 . The location of the variable p_0 singularities allows one to apply the Wick rotation procedure, although this is not justified for the variable q_0 in general.

It is convenient to start with the so-called static approximation. It assumes that all the terms in the Lorentz transformations proportional to η are canceled and the relativistic covariance for the EM current matrix element is violated. Analyzing integrands of F_{1-4} in this case, one can see that the poles on q_0 do not cross the imaginary q_0 axis and always stay in the second and fourth quadrants. Therefore, the Wick rotation procedure $q_0 \rightarrow iq_4$ can be applied.

To recover the relativistic covariance, we consider the relativistic corrections to SA. They consist of three parts. First, we calculate the Lorentz boost in the one-particle propagator $G'_1(k'_1)$ arguments, which gives a boost contribution (BC). Second, we take into account a simple pole on q_0 , which gives an additional term in integrals – a pole contribution (PC). Third, we compute the Lorentz boost of the arguments of the final trinucleon wave function by carrying out the first term of the Taylor series expansion contribution (EC) on the parameter η .

4. Results and discussion

As in the case of the rank-one kernel, we have used numerical solutions for the trinucleon amplitudes obtained by solving the system of homogeneous integral BSF equations by means of the Gaussian quadratures. The solutions mentioned above were interpolated to the (q_4, q) points of integration to perform multiple integration in equations F_{1-4} using the Vegas algorithm of the Monte-Carlo integrator. The stability of the result was tested by changing the (q_4, q) -meshes while solving the BSF equations. The best mesh was taken as $N_1 = 35, N_2 = 25$ where $N_1(N_2)$ stands for the number of $q_4(q)$ points. The multiple integrals were calculated with the relative accuracy equal to 0.01.

It should be emphasized that the considered separable covariant Graz-II kernels were obtained from the purely phenomenological nonrelativistic Graz-II potential, while the covariant Paris-1(2) kernels were received from the NR realistic one-boson-exchange Paris model.

In this section we use the dipole fit for nucleon form factors if not stated otherwise.

Now we discuss the comparison of the SA results with the ones obtained in paper [2] within the following approximation: the functions $\psi_{2,3}$ which depend on angular integration $x = \cos \theta_{qp}$ were averaged numerically while the integration in the propagators was performed analytically. The angular averaging leads to $\psi_2 = \psi_3 \sim \psi_1$ which consequently gives the following condition: $v_2 \sim 0$. To imitate the [2] calculations, we have used the analytical expressions for the propagators and taken into account the F_1 function only with the integral calculated numerically without averaging on the x variable. The obtained results are very similar to those shown in [2] but they differ from the complete calculations. The reason is that in complete integration

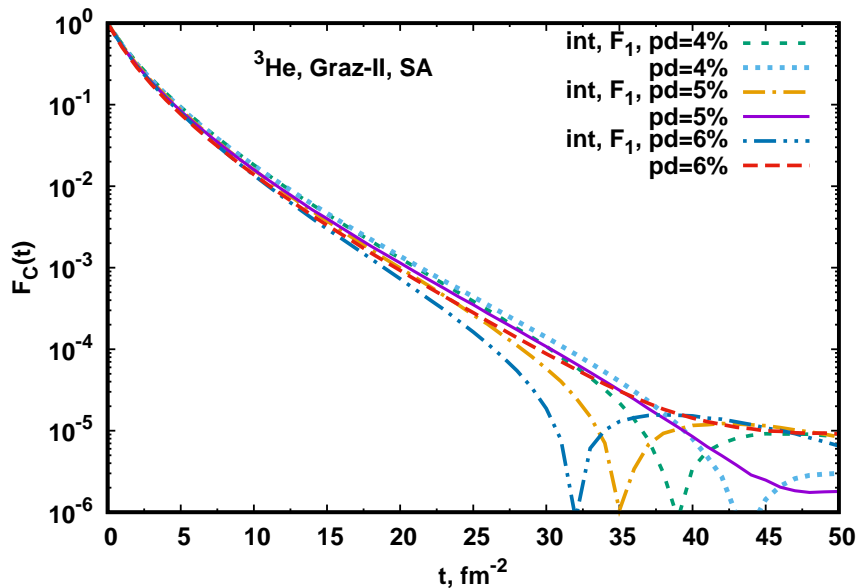


Figure 1: Static approximation for the charge form factor of ${}^3\text{He}$ as a function of t for the multirank separable kernel Graz-II at different values of the probability of the two-nucleon D -state $p_d = 4, 5, 6\%$. Complete calculations (the dotted line – for $p_d=4\%$, the solid line – for $p_d=5\%$ and the long-dashed line – for $p_d=6\%$) are compared to the [2] calculations within certain approximations (the dashed line – for $p_d=4\%$, the dashed-dotted line – for $p_d=5\%$ and the dashed-dotted-dotted line – for $p_d=6\%$).

the function v_2 is not equal to zero and gives a noticeable contribution into function F_2 which dominates in the region of the form factor zero.

Figure 1 shows the result of the calculations of the ${}^3\text{He}$ charge form factor for the cases of complete integrations and the approximation from [2] for the kernel Graz-II. As mentioned above, there is a big difference between these two assumptions. Figure 2 illustrates the same as in Figure 1 but for the Paris-1 and Paris-2 kernels.

Now we discuss the contribution of the RC to the ${}^3\text{He}$ and ${}^3\text{H}$ charge and magnetic form factors. As it is shown in [1] neither the SA nor RC calculated with the rank-one NN kernel give the diffraction minimum in the form factors. The static approximation within the multirank kernels produces the minimum/zero in the form factors which is shifted to the higher momentum transfer squared region in comparison to the experimental data. We expect the RC to shift the minimum/zero closer to the position of the

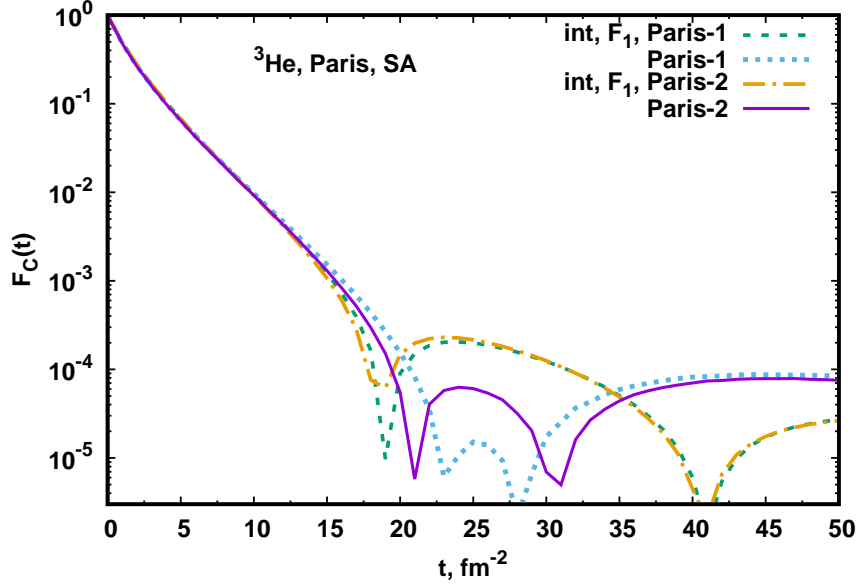


Figure 2: Static approximation for the charge form factor of ${}^3\text{He}$ as a function of t for the multirank separable kernel Paris. Complete calculations (the dotted line – for Paris-1 and the solid line – for Paris-2) are compared to the [2] calculations within certain approximation (the dashed line – for Paris-1, the dashed-dotted line – for Paris-2).

experimental data.

Figure 3 shows the partial contributions of the RC to the ${}^3\text{He}$ charge form factor, namely, the BC, PC and EC for the Graz-II multirank kernel with $p_d = 4\%$. Figure 4 illustrates the same for the Paris-1 kernel. At the low values of $t=1-2 \text{ fm}^{-2}$ the PC and EC are small due to the small corresponding value of variable η and the RC are defined by the BC. Starting approximately from $t = 5 \text{ fm}^{-2}$ the values of the BC and EC are equal to each other and their sum makes the major contribution to RC. As it is seen from the Figures above the form factor zero at value $t = 33 \text{ fm}^{-2}$ for the Graz-II kernel (at $t = 16 \text{ fm}^{-2}$ for Paris-1) is defined by zero of the EC at $t = 30 \text{ fm}^{-2}$ for Graz-II (at $t = 12 \text{ fm}^{-2}$ for Paris-1) and shifted by the positive contribution of the BC. In the region after the form factor zero the BC sharply decreases and the RC are totally determined by the EC. The PC is rather small in comparison to the BC and EC and does not play a significant role except for the case when the sum of the BC and EC is close to the value of PC at small t and near the form factor zero.

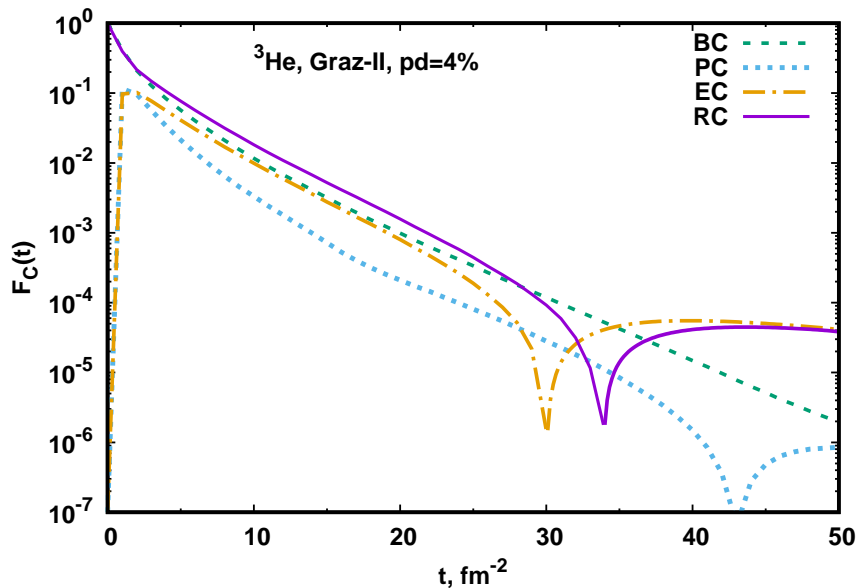


Figure 3: Parts of contribution to relativistic corrections for the ${}^3\text{He}$ charge form factor as a function of t for the multirank separable kernel Graz-II at the probability of the two-nucleon D -state $p_d = 4\%$. The solid line displays the sum of all considered relativistic corrections, the dashed line – Lorentz transformations of arguments of a propagator, the dotted line displays the contribution of the simple pole of the one-particle propagator, and the dashed-dotted line – Lorentz transformations of the arguments of the final particle wave function.

Figure 5 shows the SA and RC for the ${}^3\text{He}$ charge form factor as a function of t for the multirank separable kernel Graz-II at different values of the probability of the two-nucleon D -state $p_d = 4, 5, 6\%$. For all the curves there is a diffraction minimum/zero except for the cases of the SA with $p_d = 5, 6\%$ where the minimum without changing the sign is found. The relativistic corrections for all the values of p_d shift zeros to the region of the smaller t closer to the experimental data. The difference between the RC and experimental zeros is about $18\text{-}23 \text{ fm}^{-2}$.

Figure 6 presents the SA and RC for the ${}^3\text{H}$ charge form factor. In this case the SA gives the first form factor zero at about 40 fm^{-2} for $p_d=4\%$, 34 fm^{-2} for $p_d=5\%$ and 29 fm^{-2} for $p_d=6\%$. For all p_d values the RC shift the results closer to the experimental data of the diffraction minima in comparison to the SA. The difference between the RC and experimental zeros is less than in the ${}^3\text{He}$ charge form factor and is about $9\text{-}15 \text{ fm}^{-2}$.

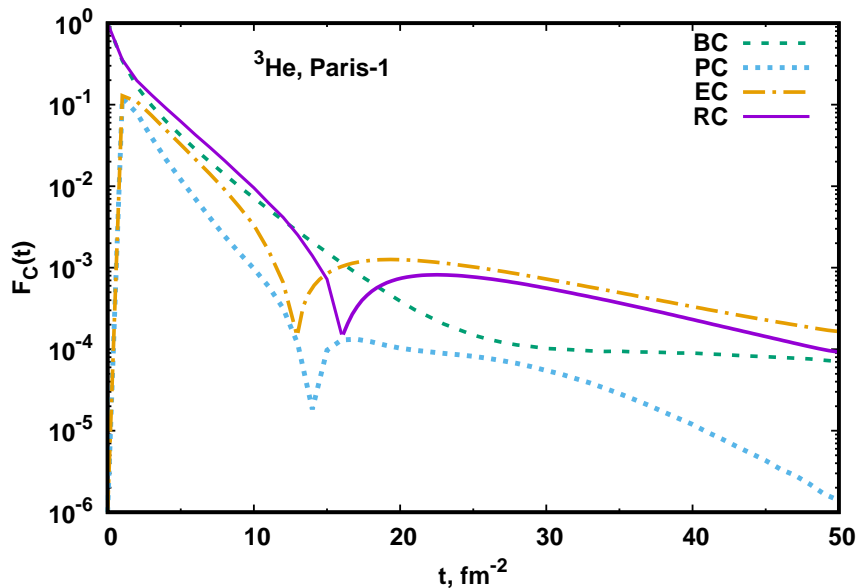


Figure 4: The same as in Fig. 3 for the multirank separable kernel Paris-1.

Figure 7 shows the SA and RC for the ${}^3\text{He}$ magnetic form factor. The results are similar to the ${}^3\text{He}$ charge form factor. However, the difference between the RC and experimental zeros is larger than in the ${}^3\text{He}$ charge form factor and is about $15\text{-}17\text{ fm}^{-2}$.

Figure 8 displays the SA and RC for the ${}^3\text{H}$ magnetic form factor. The results are similar to the ${}^3\text{H}$ charge form factor (Fig. 5). In this case the difference between the RC and experimental zeros is less than in the ${}^3\text{H}$ charge form factor and is about $2\text{-}10\text{ fm}^{-2}$ for $p_d=4,5\%$. The relativistic corrections for $p_d = 6\%$ agree with the experimental data zero and their behaviour is rather well described.

The results for the ${}^3\text{He}$ and ${}^3\text{H}$ charge and magnetic form factors with the Paris-1 and Paris-2 kernels are presented in Figures 9–12. The calculation results indicate that in this case as well as in the case of the Graz-II kernel the RC shift the curves towards the experimental data. The difference between the data and calculation results is generally smaller than for the Graz-II kernel. Figure 9 demonstrates that for the ${}^3\text{He}$ charge form factor the RC are rather close to the data zero and the difference is small – about $5(6)\text{ fm}^{-2}$ for Paris-1(2) kernels. Opposite to the ${}^3\text{He}$ charge form factor the

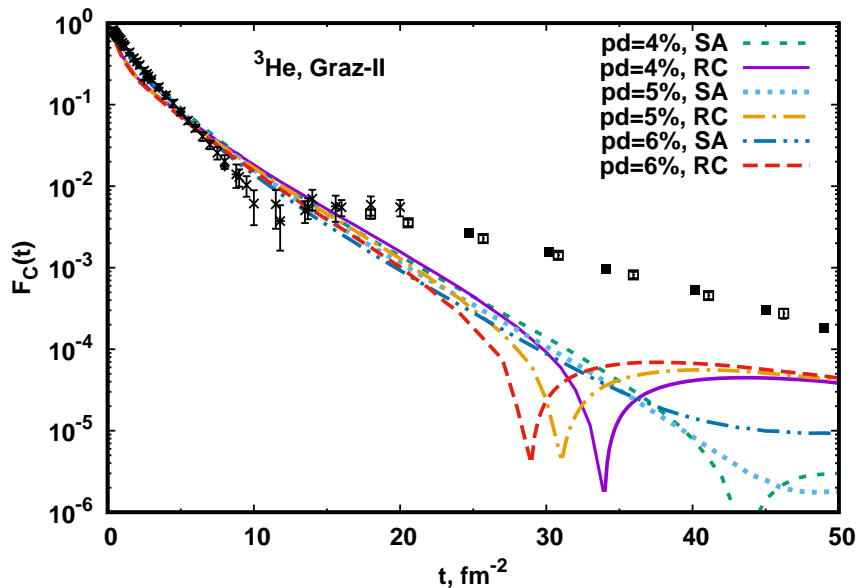


Figure 5: Static approximation and relativistic corrections for the ${}^3\text{He}$ charge form factor as a function of t for the multirank separable kernel Graz-II at different values of the probability of the two-nucleon D -state $p_d = 4, 5, 6\%$. The dashed line – SA for $p_d=4\%$, the dotted line – SA for $p_d=5\%$, the dashed-dotted-dotted line – SA for $p_d=6\%$, the solid line – RC for $p_d=4\%$, the dashed-dotted line – RC for $p_d=5\%$ and the long-dashed line – RC for $p_d=6\%$. The experimental data are taken from [14, 15, 16, 17, 18].

zero position and behaviour of the magnetic one in the region $t=16-50 \text{ fm}^{-2}$ are in rather good agreement with the experimental data (Figures 11) while the ${}^3\text{H}$ magnetic form factor the RC have zeros shifted to the smaller values of t in comparison to the data.

It should be stressed that in most cases of the above-mentioned multirank kernels (except the Paris-1(2) for ${}^3\text{He}$ and ${}^3\text{H}$ magnetic form factors) the RC also increase the value of the form factors by an order of magnitude 0.5-1.5 at the value of $t = 50 \text{ fm}^{-2}$ in comparison to the SA calculations.

Finally, we consider the contribution of different models of the nucleon EM form factors: the dipole model (DIPOLE), relativistic harmonic oscillator model (RHOM) [26] and vector meson dominance model (VMDM) [27]. The VMDM has used the latest experimental data to refit the parameters. The results for the above three models are given for the ${}^3\text{He}$ charge form factor in Fig. 13 for Graz-II and in Fig. 14 for Paris kernels. The Figures

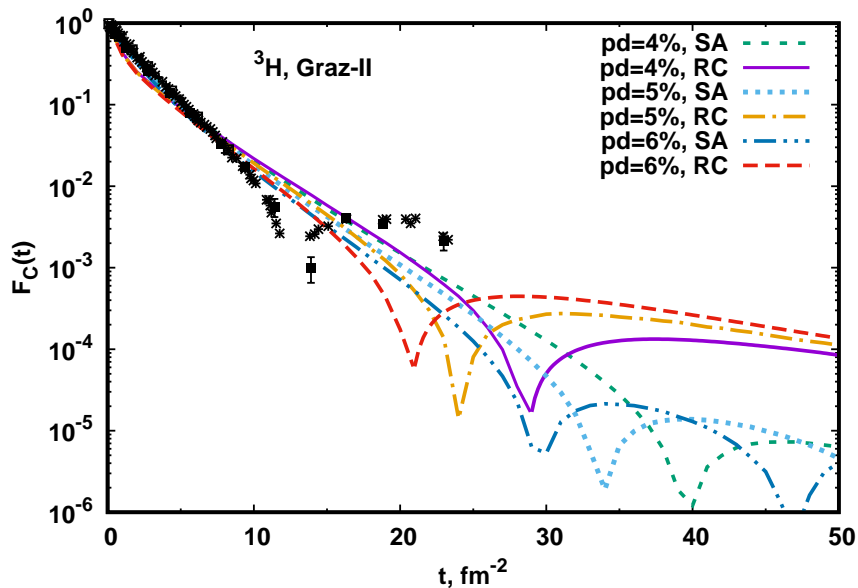


Figure 6: The same as in Fig. 5 but for the ^3H charge form factor. The experimental data are taken from [14, 22, 23, 24, 25].

demonstrate that the models change the magnitudes of the form factors by a factor of 1.5-2 at $t = 50 \text{ fm}^{-2}$ and also shift slightly the form factor zero. The main effect of the above changes happens due to the non-zero electric neutron form factor G_E^n in the RHOM and VMDM.

We have to emphasize that the considered RC are nothing but the restoration of the covariance of the trinucleon EM current matrix element although at the first order of the Taylor series expansion of the final trinucleon wave function arguments. The effect of RC is large and important as it is seen from the results. These RC change the static approximation results in the proper direction. We have calculated the relativistic impulse approximation (RIA) which takes into account only three contributions from the individual photon-nucleon diagrams and also considers the nucleon EM form factors on-mass-shell (as CIA discussed above). The RIA obviously violates the gauge invariance of the reaction. To recover this invariance, one should introduce the corresponding EM interaction currents which together with RIA provide the gauge invariance. Hopefully, this contribution will improve the agreement between the RC and experimental data.

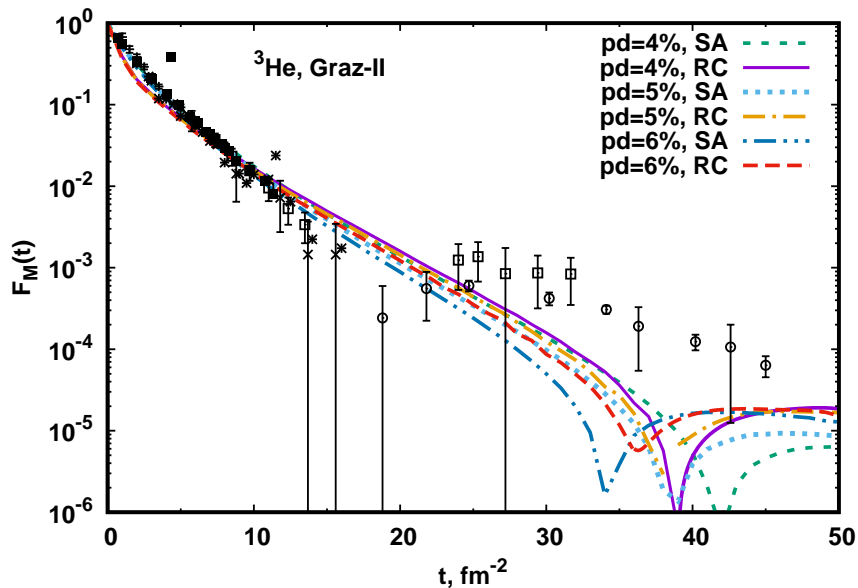


Figure 7: The same as in Fig. 5 but for the ^3He magnetic form factor. The experimental data are taken from [14, 15, 16, 18, 19, 20, 21].

5. Summary

In this paper the BSF equations solved for trinucleon have been used to calculate the trinucleon electromagnetic form factors. The expressions for the form factors have been obtained by a straightforward relativistic generalization of the NR expressions. The multiple integration has been performed by means of the Monte Carlo algorithm. The Lorentz transformations of the propagator arguments and the final trinucleon wave function have been taken into account while calculating.

The obtained solutions with multirank kernels Graz-II and Paris-1(2) unlike the rank-one kernels have given the diffraction minimum. It is important to stress that the strong dependence on the type of the NN interaction kernel has been found in the calculations.

Two approximations have been considered: the static approximation and relativistic corrections. The relativistic corrections provide the diffraction minimum in the form factors and move it in the proper direction even if it does not appear in the static approximation.

For the Graz-II with $p_d = 6\%$ and Paris-1(2) kernels a good agreement

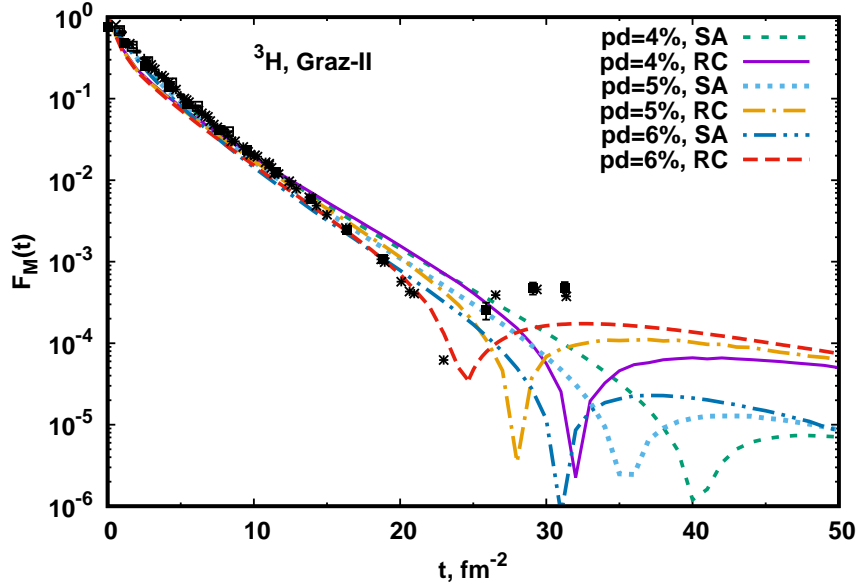


Figure 8: The same as in Fig. 5 but for the ${}^3\text{H}$ magnetic form factor. The experimental data are taken from [14, 22, 23, 24, 25].

has found for the position of the diffraction minimum in F_M of ${}^3\text{H}$ and of ${}^3\text{He}$, respectively.

Finally, we can also conclude that taking into account the EM interaction currents will be justified to provide the gauge invariance and further progress in the study of elastic electron-trinucleon scattering.

References

- [1] S. Bondarenko, V. Burov and S. Yurev, Relativistic rank-one separable kernel for helium-3 charge form factor, Nucl. Phys. A 1004 (2020) 122065. doi:10.1016/j.nuclphysa.2020.122065.
- [2] G. Rupp, J. Tjon, Bethe-Salpeter calculation of three nucleon observables with multirank separable interactions, Phys. Rev. C 45 (1992) 2133. doi:10.1103/PhysRevC.45.2133.
- [3] L. Mathelitsch, W. Plessas, W. Schweiger, Separable Potential for the Neutron Proton System, Phys. Rev. C 26 (1982) 65. doi:10.1103/PhysRevC.26.65.

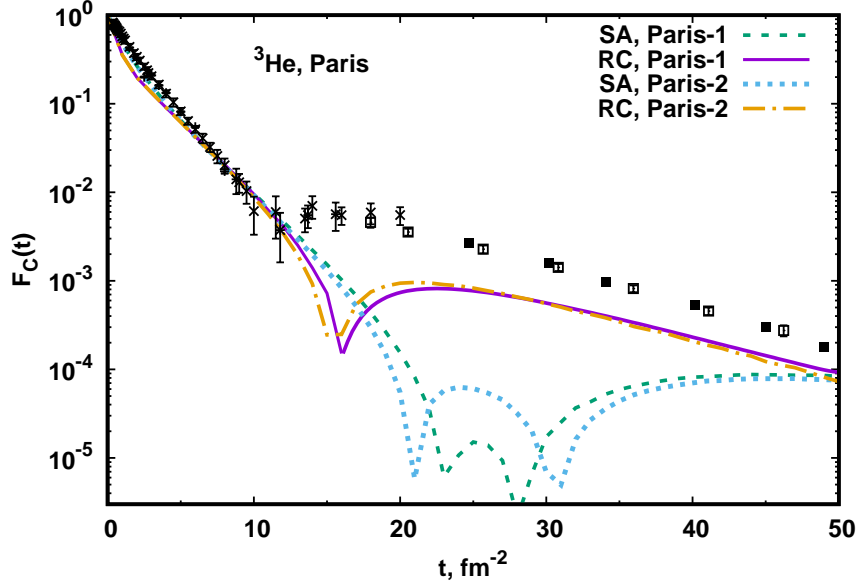


Figure 9: Static approximation and relativistic corrections for the ${}^3\text{He}$ charge form factor as a function of t for the multirank separable kernel Paris. The Dashed line – SA for Paris-1, the dotted line – SA for Paris-2, the solid line – RC for Paris-1, and the dashed-dotted line – RC for Paris-2. The experimental data coincide with Fig. 5.

- [4] J. Haidenbauer and W. Plessas, Separable representation of the Paris nucleon-nucleon potential, *Phys. Rev. C* 30 (1984) 1822. doi:10.1103/PhysRevC.30.1822.
- [5] J. Haidenbauer and W. Plessas, Modified separable representation of the Paris nucleon-nucleon potential in the S-01 and P-03 states, *Phys. Rev. C* 32 (1985) 1424. doi:10.1103/PhysRevC.32.1424.
- [6] L. Marcucci, F. Gross, M. Pena, M. Piarulli, R. Schiavilla, I. Sick, A. Stadler, J. Van Orden, M. Viviani, Electromagnetic Structure of Few-Nucleon Ground States, *J. Phys. G* 43 (2016) 023002. arXiv:1504.05063, doi:10.1088/0954-3899/43/2/023002.
- [7] F. Baroncini, A. Kievsky, E. Pace, and G. Salme, Trinucleon Electromagnetic Form Factors and the Light-Front Hamiltonian Dynamics, *AIP Conf. Proc.* 1056(1) (2008) 272–279. arXiv:0807.4809, doi:10.1063/1.3013052.

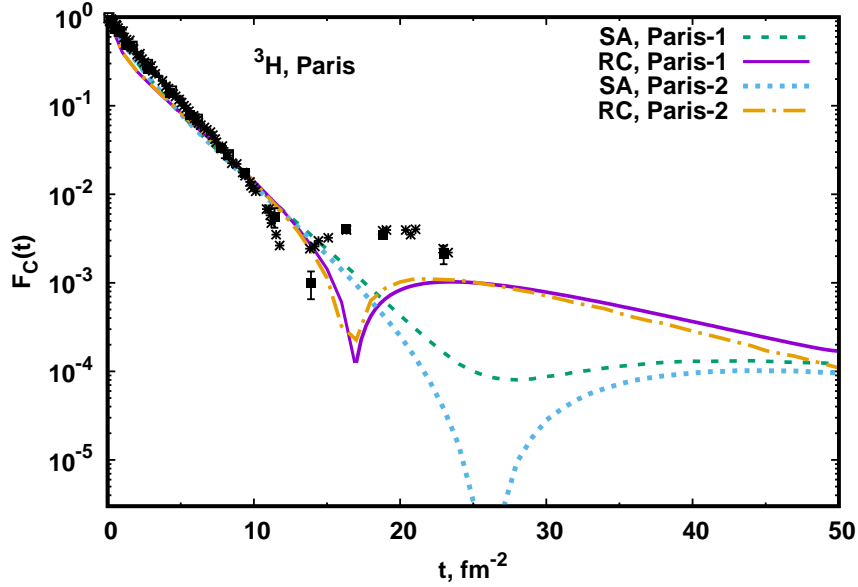


Figure 10: The same as in Fig. 9 but for the ${}^3\text{H}$ charge form factor. The experimental data coincide with Fig. 6.

- [8] A. G. Sitenko and V. F. Kharchenko, Bound states and scattering in a system of three particles, *Soviet Physics Uspekhi* 14 (1971) 125–153. doi: {10.1070/pu1971v014n02abeh004454}.
- [9] L. Schiff, Theory of the Electromagnetic Form Factors of H-3 and He-3, *Phys. Rev.* 133 (1964) B802–B812. doi:10.1103/PhysRev.133.B802.
- [10] B. Gibson, L. Schiff, P- and D-State Contributions to the Charge Form Factors of H-3 and He-3, *Phys. Rev.* 138 (1965) B26–B32. doi:10.1103/PhysRev.138.B26.
- [11] G. Rupp, J. Tjon, Bethe-Salpeter Calculation of Three Nucleon Observables With Rank One Separable Potentials, *Phys. Rev. C* 37 (1988) 1729. doi:10.1103/PhysRevC.37.1729.
- [12] S. Bondarenko, V. Burov, S. Yurev, Sensitivity of elastic electron scattering off the ${}^3\text{He}$ to the nucleon form factors, *EPJ Web Conf.* 204 (2019) 05009. arXiv:1903.01771, doi:10.1051/epjconf/201920405009.

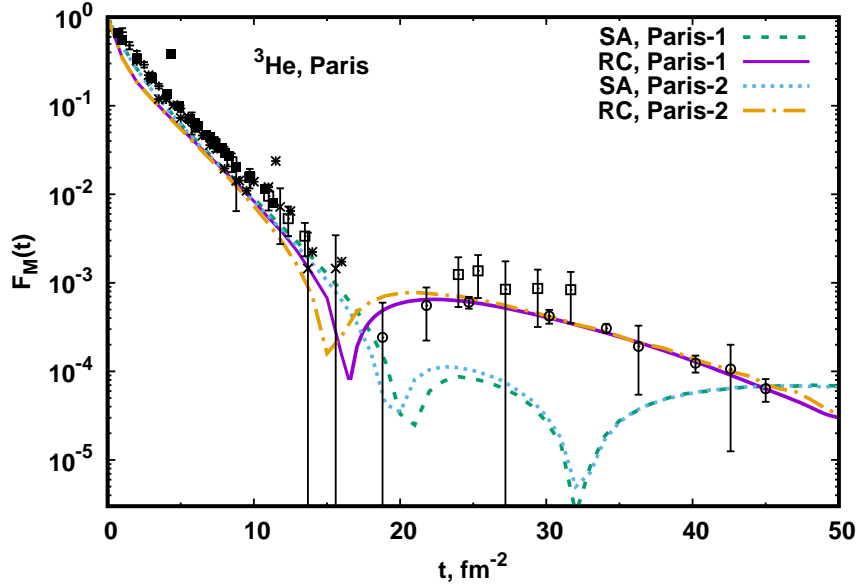


Figure 11: The same as in Fig. 9 but for the ^3He magnetic form factor. The experimental data coincide with Fig. 7.

- [13] S. Bondarenko, V. Burov, S. Yurev, On the contribution of the P and D partial-wave states to the binding energy of the triton in the Bethe-Salpeter-Faddeev approach, *Phys. Atom. Nucl.* 82 (1) (2019) 44–49. [arXiv:1809.03271](https://arxiv.org/abs/1809.03271), [doi:10.1134/S1063778819010058](https://doi.org/10.1134/S1063778819010058).
- [14] H. Collard, R. Hofstadter, E.B. Hughes, A. Johanson, M.R. Yearian, R.B. Day, and R.T. Wagner, Elastic Electron Scattering from Tritium and Helium-3, *Phys. Rev.* 138 (1965) B57. [doi:10.1103/PhysRev.138.B57](https://doi.org/10.1103/PhysRev.138.B57).
- [15] M. Bernheim, D. Blum, W. McGill, R. Riskalla, C. Trail, T. Stovall, D. Vinciguerra, Elastic electron scattering from he-3 at high momentum transfer, *Lett. Nuovo Cim.* 5S2 (1972) 431–434. [doi:10.1007/BF02905269](https://doi.org/10.1007/BF02905269).
- [16] J. McCarthy, I. Sick, R. Whitney, Electromagnetic Structure of the Helium Isotopes, *Phys. Rev. C* 15 (1977) 1396–1414. [doi:10.1103/PhysRevC.15.1396](https://doi.org/10.1103/PhysRevC.15.1396).

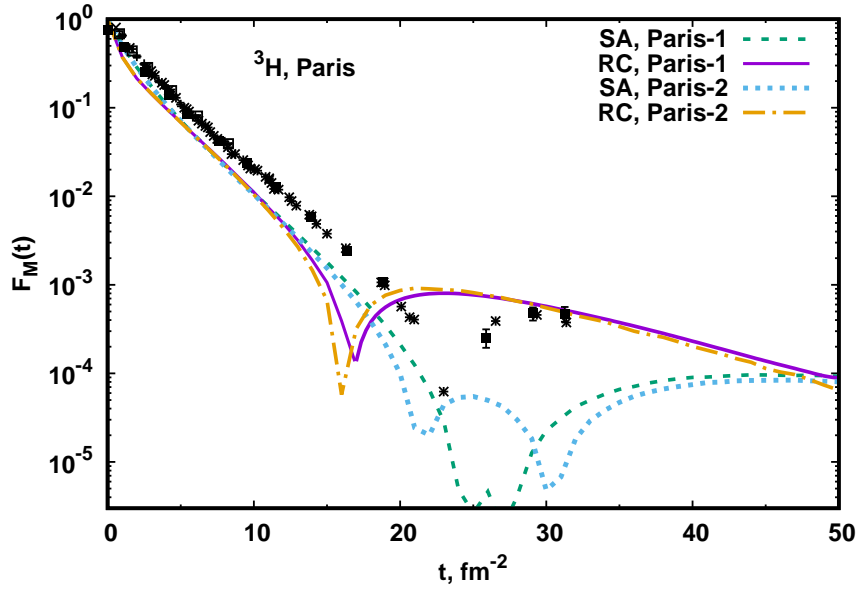


Figure 12: The same as in Fig. 9 but for the ${}^3\text{H}$ magnetic form factor. The experimental data coincide with Fig. 8.

- [17] R. Arnold, et al., Elastic electron Scattering from He-3 and He-4 at High Momentum Transfer, *Phys. Rev. Lett.* 40 (1978) 1429. doi:10.1103/PhysRevLett.40.1429.
- [18] A. Camsonne, et al. (The Jefferson Lab Hall A Collaboration), JLab Measurements of the ${}^3\text{He}$ Form Factors at Large Momentum Transfers, *Phys. Rev. Lett.* 119 (16) (2017) 162501, [Addendum: *Phys.Rev.Lett.* 119, 209901 (2017)]. arXiv:1610.07456, doi:10.1103/PhysRevLett.119.162501.
- [19] J. M. Cavedon, B. Frois, D. Goutte, M. Huet, Ph. Leconte, J. Martino, X. -H. Phan, S. K. Platchkov, S. E. Williamson, W. Boeglin, I. Sick, P. de Witt-Huberts, L. S. Cardman, and C. N. Papanicolas Magnetic Form Factor of ${}^3\text{He}$ *Phys. Rev. Lett.*, 49 (1982) 986. doi:10.1103/PhysRevLett.49.986.
- [20] P. C. Dunn, S. B. Kowalski, F. N. Rad, C. P. Sargent, W. E. Turchinetz, R. Goloskie, and D. P. Saylor, ${}^3\text{He}$ magnetic form factor, *Phys. Rev. C*

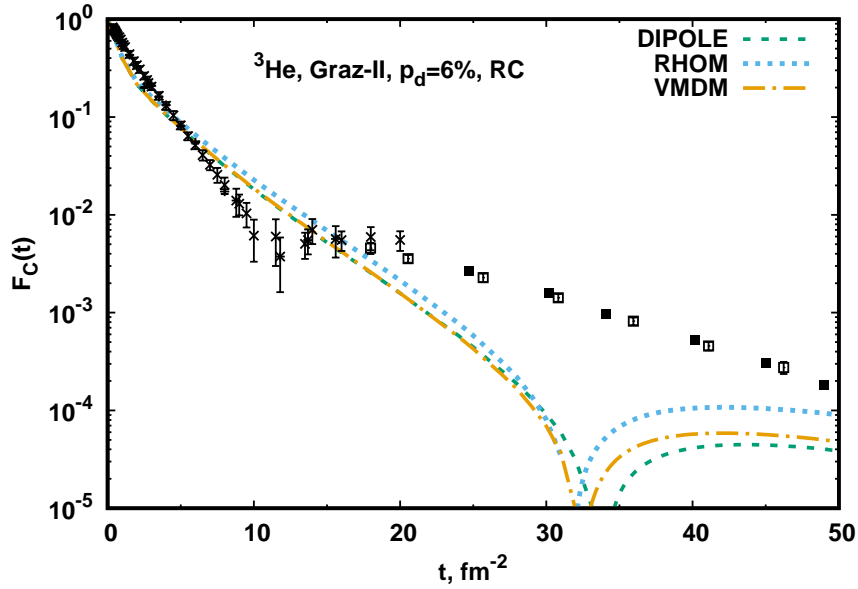


Figure 13: Relativistic corrections to the ${}^3\text{He}$ charge form factor for Graz-II ($p_d = 4\%$) kernel with three models of the EM nucleon form factors: the dashed line - DIPOLE, the dotted line - RHOM, the dashed-dotted line - VMDM. The experimental data coincide with Fig. 8.

27 (1983) 71. <https://doi.org/10.1103/PhysRevC.27.71> doi:10.1103/PhysRevC.27.71.

- [21] I. Nakagawa, J. Shaw, S. Churchwell, X. Jiang, B. Asavapibhop, M. C. Berisso, P. E. Bosted, K. Burchesky, F. Casagrande, A. Cichocki, R. S. Hicks, A. Hotta, T. Kobayashi, R. A. Miskimen, G. A. Peterson, S. E. Rock, T. Suda, T. Tamae, W. Turchinetz, and K. Wang Measurement of the Elastic Magnetic Form Factor of ${}^3\text{He}$ at High Momentum Transfer Phys. Rev. Lett. 86 (2001) 5446. doi:10.1103/PhysRevLett.86.5446.
- [22] D. H. Beck, S. B. Kowalski, M. E. Schulze, W. E. Turchinetz, J. W. Lightbody, Jr., X. K. Maruyama, W. J. Stapor, H. S. Caplan, G. A. Retzlaff, D. M. Skopik, and R. Goloskie, Tritium form factors at low q , Phys. Rev. C 30 (1984) 1403. <https://doi.org/10.1103/PhysRevC.30.1403> doi:10.1103/PhysRevC.30.1403.
- [23] F.P. Juster, S. Auffret, J.-M. Cavedon, J.-C. Clemens, B. Frois,

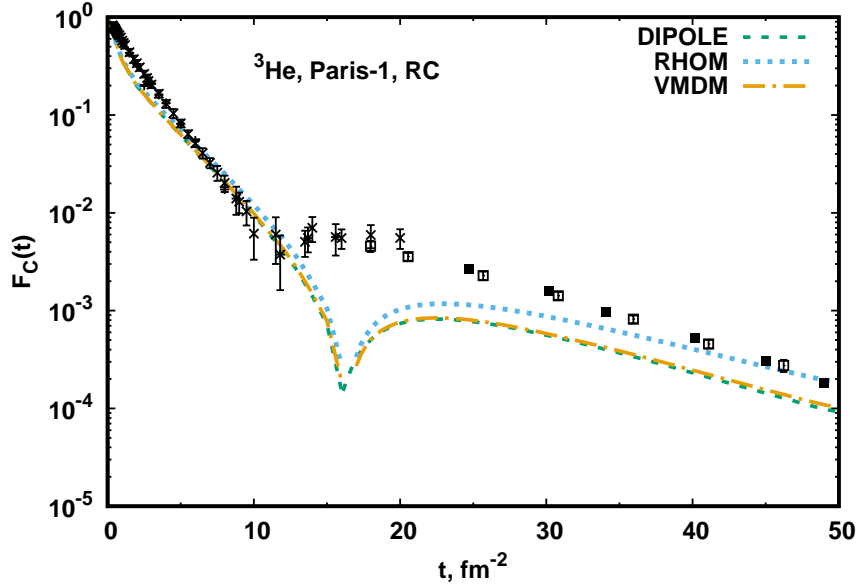


Figure 14: The same as in Fig. 13 but for the Paris-1 kernel.

D. Goutte, M. Huet, P. Leconte, J. Martino, Y. Mizuno, X.-H. Phan, S. Platchkov, S. Williamson, and I. Sick, Tritium electromagnetic form-factors, *Phys. Rev. Lett.*, 55 (1985) 2261. doi:10.1103/PhysRevLett.55.2261.

- [24] D. Beck, A. Bernstein, I. Blomqvist, H. Caplan, D. Day, P. Demos, W. Dodge, G. Dodson, K. Dow, S. Dytman, M. Farkhondeh, J. Flanz, K. Giovanetti, R. Goloskie, E. Hallin, E. Knill, S. Kowalski, J. Lightbody, R. Lindgren, X. Maruyama, J. McCarthy, B. Quinn, G. Retzlaff, W. Sapp, C. Sargent, D. Skopik, I. The, D. Tieger, W. Turchinets, T. Ueng, N. Videla, K. von Reden, R. Whitney, D. Skopik, and C. Williamson, Isoscalar and isovector form factors of H-3 and He-3 for Q below 2.9 fm⁻¹ from electron-scattering measurements, *Phys. Rev. Lett.*, 59 (1987) 1537. doi:10.1103/PhysRevLett.59.1537.
- [25] A. Amroun, V. Breton, J.M. Cavedon, B. Frois, D. Goutte, F.P. Juster, Ph. Leconte, J. Martino, Electromagnetic Structure of Few-Nucleon Ground States 64 Y. Mizuno, X.-H. Phan, S.K. Platchkov, I. Sick, and

- S. Williamson, H-3 and He-3 electromagnetic form-factors, Nucl. Phys. A, 579 (1994) 596. doi:10.1016/0375-9474(94)90925-3.
- [26] V. V. Burov, A. De Pace, S. M. Dorkin, and P. Saracco, Hadron and quark form-factors in the relativistic harmonic oscillator model, Europhys. Lett. 24 (1993) 443–448. doi:10.1209/0295-5075/24/6/003.
- [27] R. Bijker, and F. Iachello, Re-analysis of the nucleon space- and time-like electromagnetic form-factors in a two-component model, Phys. Rev. C69 (2004) 068201. doi:10.1103/PhysRevC.69.068201.

